Theor Chem Acc (2014) 133:1531
DOI 10.1007/s00214-014-1531-4

REGULAR ARTICLE

DFT and TD-DFT studies on osmacycle dyes with tunable photoelectronic properties for solar cells

Mingjun Sun · Zexing Cao

Received: 3 June 2014 / Accepted: 26 June 2014 / Published online: 5 July 2014

Abstract B3LYP and CAM-B3LYP functionals have been used to determine structures, electronic and optical properties of osmium-bridged tricyclic aromatic compounds. Calculations show that the optical properties and charge separation features of these osmacycle derivatives can be well modified by incorporating different π-bridge groups. In particular, the newly designed osmacycle dyes **5** and **6** by embedding thiophene and thienothiophene bridge units to osmium polycyclic aromatic system show very strong and broad adsorptions in the whole visible region and excellent charge separation in the first excited state of $^1(\pi\pi^*)$ from the hightest occupied molecular orbital to the lowest unoccupied molecular orbital excitation. Furthermore, the predicted relatively high light harvesting efficiency and large driving force for electron injection suggest that they are quite promising for design of high-performance dye-sensitized solar cells.

Keywords Metal-bridged tricyclic aromatic systems · Density functional calculations · Osmacycle dyes · Structural modification · Absorption spectra · Electron injection

Dedicated to Professor Guosen Yan and published as part of the special collection of articles celebrating his 85th birthday.

Electronic supplementary material The online version of this article (doi:10.1007/s00214-014-1531-4) contains supplementary material, which is available to authorized users.

M. Sun · Z. Cao (✉)
State Key Laboratory of Physical Chemistry of Solid Surfaces and Fujian Provincial Key Laboratory of Theoretical and Computational Chemistry, College of Chemistry and Chemical Engineering, Xiamen University, Xiamen 361005, China
e-mail: zxcao@xmu.edu.cn

1 Introduction

Solar power plays an important role in turning energy systems toward sustainability. Among the photovoltaic devices, the dye-sensitized solar cell (DSSC) is the only solar device that mimics the photosynthesis process in a green leaf. Owing to its simplicity of manufacturing process, low cost, and relatively high energy conversion efficiency, DSSCs become the promising one of renewable energy devices [1, 2]. In general, DSSC is composed of five components, including conductive mechanical support, semiconductor film, sensitizer, electrolyte containing I^-/I_3^- redox couple and counter electrode with a trioxide reduction catalyst [3–6]. As one of the crucial parts in DSSCs, the photosensitizer to harvest sunlight has been viewed as a breakthrough for performance improvement of DSSCs.

Since O'Regan and Grätzel reported the first successful DSSC based on the mechanism of a fast regenerative photoelectrochemical process in 1991, the design of high-performance sensitizers has attracted considerable attention, both experimentally and theoretically [3–20, 29, 41, 46–48], in order to enhance the power conversion efficiency (PCE) of DCCSs. High-efficient dyes commonly should fulfill some essential requirements, including the broad absorption ranging from the whole visible region to the near-infrared part, the novel anchoring groups with strong adsorption on the semiconductor surface, the adaptation of corresponding energy levels among the conduction edge of semiconductor, the excited-state and oxidized-state levels of dyes, and the redox potential of electrolyte, as well as high electrochemical and thermal stability.

At present, among widely used metal–organic and metal-free organic sensitizers for DSSCs [7], the metal-free organic dyes such as coumarin, indoline, cyanine, triphenylamine, and porphyrin have attracted considerable interest for renewable energy devices because of their significant advantages in terms of synthesis procedures, diversiform structures, and low costs [8–12]. However, the PCE for the metal–organic dyes has been recently climbed to 12.3 % [13, 14]. Among the numerous metal–organic dyes, ruthenium dyes, such as Ru bipyridine complex (red dye) [15] and Ru terpyridine complex (black dye) [16], have been extensively investigated [17, 18], and at the same time, the Os terpyridine complex was also examined for comparison. As a consequence, the osmium compounds exhibit extremely broad UV–Vis absorption, perfectly reversible electrochemistry, and prominent photochemical stability, although they suffer from lower V_{oc} or J_{sc} values under different conditions [19, 20].

Very recently, a series of novel metal-bridged polycyclic aromatic compounds have been successfully synthesized, and they show outstanding stability and unusual optical property [21–23]. To have an insight into their photoelectronic properties and possible applications in DSSCs, herein extensive density functional calculations have been performed. Based on calculations, electronic and structural properties, as well as structural modification effects on charge separation and light harvesting ability of the osmium metallacycle dyes, have been discussed.

2 Computational details

2.1 Theoretical background

It is well known that the performance of DSSCs can be characterized by the overall power conversion efficiency (η) and the monochromatic incident photo-to-electron power conversion efficiency (IPCE). The power conversion efficiency is generally defined as the ratio of the maximum solar power, P_{max}, and the incident solar power on the cell, P_{inc}, and it can be obtained by the following equation [5, 24]:

$$\eta = \frac{P_{\max}}{P_{\mathrm{inc}}} = \frac{I_{\max}\cdot V_{\max}}{P_{\mathrm{inc}}} = \frac{J_{\max}\cdot V_{\max}\cdot S}{P_{\mathrm{inc}}} = \frac{\mathrm{FF}\cdot J_{\mathrm{sc}}\cdot V_{\mathrm{oc}}\cdot S}{P_{\mathrm{inc}}} = \frac{\mathrm{FF}\cdot J_{\mathrm{sc}}\cdot V_{\mathrm{oc}}}{I_{\mathrm{s}}} \quad (1)$$

where J_{sc} is the short-circuit current density, V_{oc} is the open-circuit photovoltage, FF is the fill factor of the cell, I_s is the intensity of the incident light, and J_{max} and V_{max}, respectively, are the photocurrent density and photovoltage under the maximum solar power. The fill factor ranging from 0 to 1 is the ration of the maximum power (P_{max}) and the product of the open-circuit voltage (V_{oc}) and the short-circuit current (I_{sc}), exhibiting the extent to which the power is lost due to ohmic resistance and overpotential. According to Eq. 1, manipulation of J_{sc} and V_{oc} is an effective way to enhancement of η.

The photocurrent density, J_{sc}, is defined by integrating IPCE(λ) over the solar spectral density, $I_s(\lambda)$:

$$J_{\mathrm{sc}} = e\int \mathrm{IPCE}(\lambda) I_{\mathrm{s}}(\lambda)\mathrm{d}\lambda \quad (2)$$

$$\mathrm{IPCE}(\lambda) = \frac{n_{\mathrm{e}}}{n_{\mathrm{p}}} = \mathrm{LHE}(\lambda)\times \Phi_{\mathrm{inject}}\times \eta_{\mathrm{collect}}\times \eta_{\mathrm{reg}} \quad (3)$$

where LHE(λ) is the light harvesting efficiency at a given wavelength, Φ_{inject} is the electron injection efficiency, $\eta_{collect}$ is the charge collection efficiency at the conducting glass substrate, and η_{reg} is the dye regeneration efficiency, and therein LHE(λ) and Φ_{inject} affect prominently on IPCE(λ). LHE(λ) can be expressed as:

$$\mathrm{LHE}(\lambda) = 1 - 10^{-f} \quad (4)$$

where $A(f)$ is the absorption (oscillator strength) of the dye at the maximum wavelength [25], and the oscillator strength associated with the λ_{max}^{ICT} can be written as:

$$f = \frac{2}{3}\lambda_{\max}^{\mathrm{ICT}}|\vec{\mu}_0 - \mathrm{ICT}|^2 \quad (5)$$

Hence, f is determined by the maximum wavelength λ_{max}^{ICT} (ICT: intramolecular charge transfer) and the dipolar transition moment $|\vec{\mu}_0 - \mathrm{ICT}|$ associated with the electronic excitation [26, 27].

The electron injection efficiency Φ_{inject} is in direct proportion to the driving force (ΔG_{inject}) of the electron injection from the photoinduced excited states of sensitizer to semiconductor surface, and it can be expressed as (in eV) [28]:

$$\Delta G_{\mathrm{inject}} = E_{\mathrm{ox}}^{\mathrm{dye}*} - E_{\mathrm{CB}}^{\mathrm{TiO_2}} \quad (6)$$

where E_{ox}^{dye*} is the oxidation potential of the dye in the excited state, and $E_{CB}^{TiO_2}$ is the bottom of conduction band of titanium dioxide whose experimental value is considered as −4.0 eV [29]. As for E_{ox}^{dye*}, it was assumed that the electron injection occurs from the unrelaxed excited state because the primary electron transfer event in DSSCs is much faster than the vibrational relaxation of the photoexcited dyes [28], and E_{ox}^{dye*} can be computed as:

$$E_{\mathrm{ox}}^{\mathrm{dye}*} = E_{\mathrm{ox}}^{\mathrm{dye}} - \lambda_{\max} \quad (7)$$

λ_{max} is the vertical transition energy which is the approximation of the 0–0 transition energy E_{0-0} [28, 30], and E_{ox}^{dye} is the redox potential of the ground state of the dye which can be estimated by the Nernst equation and can also be written in the energy scale as Eq. 8.

$$E_{\mathrm{ox}}^{\mathrm{dye}} = \Delta G_{(\mathrm{aq})}/nF \quad (8)$$

The value of $\Delta G_{(aq)}$ is Gibbs free energy change due to the oxidation of the dye in solution, and it can be

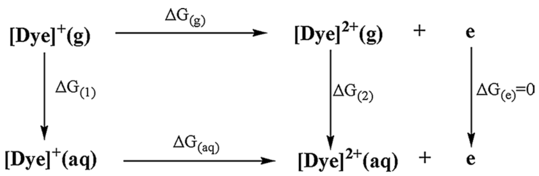

Scheme 1 Thermodynamic cycle for calculation of redox potentials

calculated according to the Born–Haber cycle, as shown in Scheme 1, where F represents the Faraday constant of 96,485.3 C mol^{-1}, and n is the number of electrons involved in the redox couple $[dye]^{2+}/[dye]^+$ (here $n = 1$) [31, 32].

2.2 Computational methods

Here, theoretical calculations of geometries, frequencies, electronic structures, as well as electronic absorption spectra for the osmapentalyne derivatives have been performed by the B3LYP functional [33, 34] with the basis sets of LANL2DZ for Os and P atoms and the 6-31G(d) basis set for other atoms implemented in Gaussian09 package [35]. Polarization functions of P ($\zeta(d) = 0.340$), S($\zeta(d) = 0.421$), and Os ($\zeta(d) = 0.886$) [36] are also added to the LANL2DZ basis set. The solvent effects of dichloromethane used in experiment have been considered using the SMD continuum solvation model [37]. Previous time-dependent density functional theory (TD-DFT) assessment suggested that the hybrid functionals of B3LYP, CAM-B3LYP, M06-2X, and PBE0 are suitable for the optical 0–0 transition of dyes in solution [30]. The coulomb-attenuating method CAM-B3LYP functional taking long-range correction into account has been proved to be appropriate for electronic excitations with character of charge transfer (CT), but the conventional exchange–correlation functional such as B3LYP is also practicable for some complexes [38–42]. Herein TD-DFT calculations with both CAM-B3LYP and B3LYP functionals were used for determination of the vertical excitation energies and corresponding oscillator strengths. In order to reduce computational costs, the triphenylphosphine ligand in the experimental complex is replaced by the phosphine (PH_3), and test calculations indicate that such simplification of ligands has only negligible influences on the structural and electronic properties of the relatively large metallacycles.

3 Results and discussion

3.1 Structural and optical properties of osmium polycyclic aromatic complexes

The geometry and absorption spectrum of the osmium-bridged tricyclic aromatic compound **1** were determined by B3LYP calculations. The optimized structure and selected bond lengths are shown in Fig. S1 and Table S1 in Supporting Information). As shown in Table S1, the B3LYP-predicted bond lengths of complex **1** with the 6-31G(d) basis set are similar with those obtained with the relatively large 6-311++G(d,p) basis set, and they are all consistent with the experimental values. Furthermore, the B3LYP/6-31G(d)-predicted strong absorptions at 350, 378, 421, and 549 nm can reasonably match the experimental bands at 353, 367, 407, and 557 nm, respectively, as shown in Fig. S2. Accordingly, the B3LYP functional with the 6-31G(d) basis set is practicable for this kind of osmium polycyclic aromatic systems.

Among the most recently synthesized osmium polycyclic aromatic systems [23], the complex with an oxygen heterocycle (**2′** in Fig. 1) was found to have strong and broad adsorptions in almost whole visible region, suggesting that it may be of high potential for the photosensitizer in solar cells, and this osmium tricyclic aromatics **2′** served as a parent was considered for subsequently computational design of osmacycle dyes.

Here, DFT calculations show that the osmacycle complex **2** from substitution of PH_3 for PPh_3 groups in **2′** has the singlet ground state, like **2′**. As shown in Fig. 1 and Table 1, both complexes **2** and **2′** have quite similar geometries, lending support to simplification of PPh_3 ligands in calculation. In particular, all predicted Os–C bond lengths in **2** (2.062–2.190 Å) as well as **2′** (2.062–2.208 Å) are within the range of Os–C single- and double-bond lengths, in which Os1–C27 (2.190 Å), Os1–C7 (2.098 Å), and Os1–C12 (2.135 Å) bear more single-bond character, while Os1–C16 (2.062 Å) has partial character of double bond [43]. Their corresponding Wiberg bond indices of **2** are 0.761, 0.894, 0.779, and 0.912, respectively. The natural charge populations at atoms Os1, C7, C12, C16, and C27 are −1.337, −0.180, −0.115, 0.432, and −0.118, respectively. Therein the relatively large natural positive charges at C16 may stem from the adjoining oxygen with large electronegativity. The dihedral angles of C27–C16–C7–C10, C22–Os1–C13–C9 are 177.6° and 178.2°, respectively, and thus complex **2** has an approximately planar conformation.

The canonical molecular orbital nucleus-independent chemical shift (CMO-NICS) analyses [44] indicate that NICS(1) values at the center of A, B, and C rings (see Scheme S1 and Table S2) are −4.3, −6.1, and −9.0 ppm, respectively. Such negative NICS values reveal the presence of notable aromaticity in this metallacycle from extending π conjugation interaction, which may play an important role in stabilizing metal-bridged tricyclic aromatic complexes.

The hightest occupied molecular orbital (HOMO) and the lowest unoccupied molecular orbital (LUMO) are generally responsible for the strong electronic transition

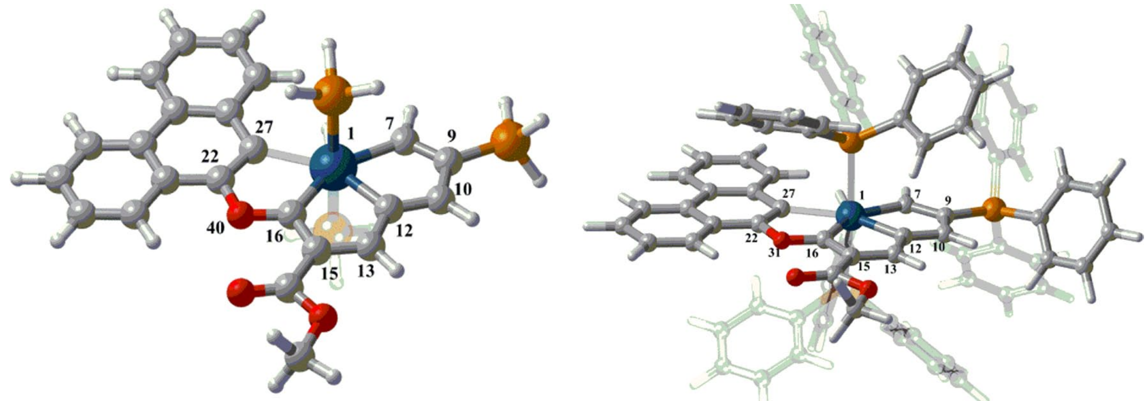

Fig. 1 Optimized structures of osmium-bridged tricyclic aromatic compounds **2** and **2′** in dichloromethane solution

Table 1 Selected predicted bond lengths (Å), bond angles (°), dihedral angels (°), charge populations, and Wiberg bond indexes (WBI) of **2** and **2′** (in parenthesis)

Bonds		Angles/dihedral angles		Charge		WBI	
Os1–C7	2.098 (2.107)	C7–Os1–C12	74.3 (73.3)	Os1	−1.337 (−1.160)	Os1–C7	0.8942 (0.9006)
Os1–C12	2.135 (2.126)	C12–Os1–C16	73.7 (73.5)	C7	−0.180 (−0.199)	Os1–C12	0.7791 (0.7740)
Os1–C16	2.062 (2.062)	C16–Os1–C27	74.1 (73.9)	C12	−0.115 (−0.131)	Os1–C16	0.9122 (0.9176)
Os1–C27	2.190 (2.208)	C27–C16–C7–C10	177.6 (179.7)	C16	0.432 (0.423)	Os1–C27	0.7614 (0.7427)
		C22–Os1–C13–C9	178.2 (178.0)	C27	−0.118 (−0.132)		

from the ground state to the first excited state. To understand the nature of absorption spectra, the electron density differences between the first excited state and the ground state and distribution of related molecular orbitals were discussed. The electron density diagrams and energies of selected frontier molecular orbitals of the complex **2** in dichloromethane solution are displayed in Fig. 2. As Fig. 2 shows, the energy levels of HOMO and LUMO are −5.20 and −2.32 eV, respectively, indicating that the HOMO–LUMO excitation may occur in the visible region.

The orbital composition analysis shows that HOMO is mainly localized over the phenanthrene moiety, while LUMO is contributed by the metal-bridged blended five membered rings in **2**. As shown in Fig. 3b, the electron densities are significantly depleted at the phenanthrene group, whereas there are increases at the metal-bridged tricyclic moiety, resulting in partial charge transfers as the electronic transition occurs from the ground state to the first excited state.

Absorption spectra of complexes **2** and **2′** in dichloromethane solution were investigated by both TD-B3LYP and TD-CAM-B3LYP calculations with the SMD solvation model, and experimental and theoretical absorption spectra are displayed in Fig. 3a. Experimentally, the dominant absorptions appear at 397 and 541 nm for complex **2′** [21–23], respectively. TD-B3LYP calculations indicate that the electronic absorptions at 396 and 529 nm have relatively large oscillator strengths of 0.11 and 0.13, respectively, showing good agreement with the experimental observations. We note that here TD-CAM-B3LYP calculations systematically overestimate the transition energies, as shown in previous studies [26]. However,

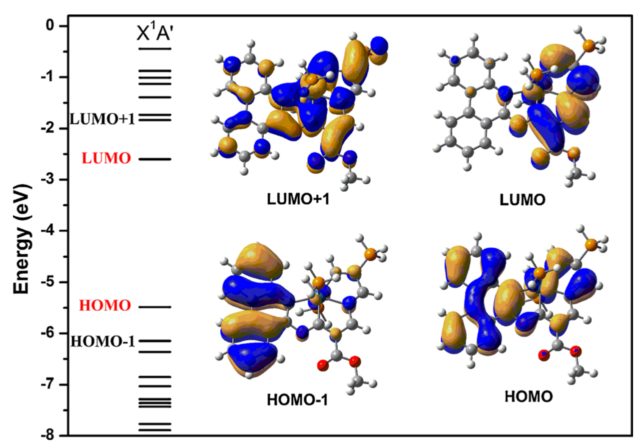

Fig. 2 Selected key frontier molecular orbitals and energy levels in the complex **2**

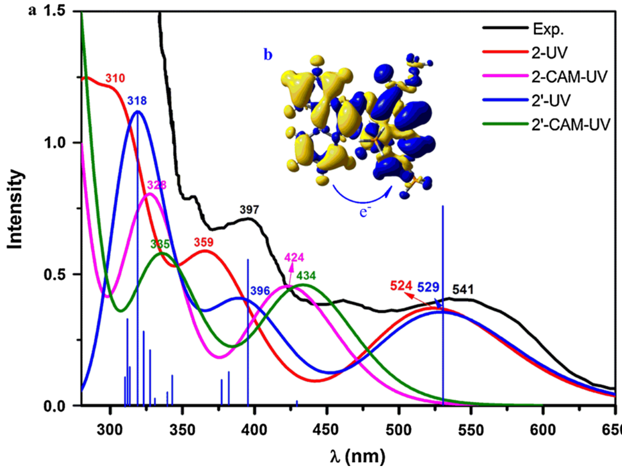

Fig. 3 **a** Electronic absorption spectra of **2** and **2′** predicted by TD-B3LYP and TD-CAM-B3LYP in dichloromethane solution; **b** Electron density differences between the first excited state and the ground state of the osmacycle **2** (*Yellow* and *blue* refer to a decrease and an increase in electron density, respectively; isovalue: 0.0004 au.)

the TD-CAM-B3LYP-predicted spectra nicely match the experimental bands both in peak positions and relative intensities if a redshift of 0.57 eV is introduced to the TD-CAM-B3LYP spectrum (refer to Fig. S3). Hence, both B3LYP and CAM-B3LYP approaches have been applied to simulation of UV/Vis spectra in following calculations. As Fig. 3a shows, the absorption spectra of complexes **2** and **2′** are similar and they all have broad absorptions in the visible region. Accordingly, the ligand-simplified complex **2** is also promising for design of high-performance dyes through introduction of various π-bridge-conjugated groups and anchoring groups.

3.2 Effects of structural modification on electronic and optical properties

To have an insight into effects of structural modification on charge separation and light harvesting ability, here four metal-bridged tricyclic aromatic derivatives in Scheme 2 have been considered, which are derived from the embedding of various π-bridge-conjugated groups to the complex **2**, based on previous studies [41, 45–47]. Considering the direction of charge transfer, the steric effect of triphenylphosphine groups, and the features of frontier orbitals, the C10 site in **2** was served as the π-bridge junction. Predicted electronic and light harvesting properties related to the dye performance are collected in Table 2. The electron density differences between the first excited state and the ground state calculated by Multiwfn [48], and distributions of HOMO and LUMO orbitals in dyes **3–6** are presented in Fig. 4 and Fig. S4, respectively.

We note that the donor (D) moiety has dominant contribution to HOMO orbitals, while the π-bridge (**B**) and the acceptor (A) groups dominate the LUMO orbitals in dyes **3–6** here. The predicted electron density differences in Fig. 4 show that the electronic densities in the donor moiety decrease remarkably, while sharp increases appear in the bridge and acceptor moieties in the low-lying states from the $S_0 \rightarrow S_1$ transition in **3–6**. This suggests that introduction of the electron-deficient pyrimidine and electron-rich thiophene bridges can further facilitate charge separation during the electronic transition in the dyes **3–6**, compared to **2**.

As Fig. 5 shows, the osmacycle **3–6** have much stronger and broad absorptions in the visible region, compared to the complex **2**. In particular, the newly designed dyes **5** and **6** containing thiophene and thienothiophene units exhibit very strong absorptions in the whole visible region. These novel spectroscopic features are highly required for enhancement of the light harvesting ability of dyes and improvement of the performance of DSSCs.

The predicted transition energies, corresponding oscillator strengths, the light harvesting efficiency LHE(λ), and the driving force $\Delta G_{\mathrm{inject}}$ are compiled into Table 2. The CAM-B3LYP functional is proved to be appropriate for the charge-transfer (CT) excitations, and it has been used to determine the vertical energies and the oscillator strengths within the TD-DFT framework. In Table 2, all strongest $S_0 \rightarrow S_1$ transitions are generally mainly contributed by the HOMO–LUMO excitation, and the first excited state is characterized by $^1(\pi\pi^*)$.

Here, all LUMO energy levels of these dyes are more positive than the bottom of conduction band of TiO_2

Scheme 2 Molecular structures of osmacycle dyes **3–6**

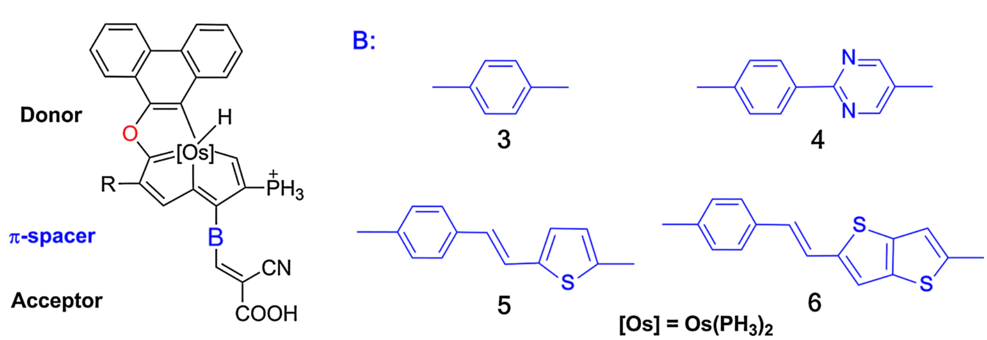

Table 2 HOMO and LUMO energies (eV), transition energies (λ in nm), corresponding oscillator strengths (*f*), the light harvesting efficiency (LHE), redox potentials (ΔE^{dye} in eV), and the driving force (ΔG_{inject} in eV) for osmacycle dyes by B3LYP and CAM-B3LYP

Dye	HOMO/LUMO	λ_{max}	Main configurations	*f*	LHE	ΔE^{dye}	ΔG_{inject}
B3LYP							
1	−5.15/−2.49	549	H → L(0.70)	0.33	0.53	4.96	−1.30
2	−5.20/−2.32	529	H → L(0.69)	0.13	0.26	5.23	−1.11
2′	−5.48/−2.60	524	H → L(0.69)	0.14	0.28	4.98	−1.39
3	−5.51/−3.02	595	H → L(0.69) H-1 → L(0.12)	0.37	0.57	5.31	−0.77
4	−5.48/−3.11	603	H → L(0.68) H → L + 1(0.19)	0.38	0.58	5.24	−0.81
5	−5.44/−2.99	590	H → L(0.66) H → L + 1(0.24)	0.77	0.83	5.29	−0.81
6	−5.43/−2.99	591	H → L(0.65) H → L + 1(0.26)	1.03	0.91	5.27	−0.82
CAM-B3LYP							
1	−6.31/−1.32	431	H → L(0.58) H-1 → L(0.32)	0.53	0.70	5.11	−1.76
2	−6.44/−1.17	434	H → L(0.63) H-1 → L(0.14)	0.17	0.32	5.32	−1.54
2′	−6.70/−1.41	424	H → L(0.62) H → L + 1(0.15)	0.17	0.32	5.16	−1.76
3	−6.71/−1.83	448	H → L(0.55) H → L + 1(0.32)	0.45	0.65	5.68	−1.08
4	−6.68/−1.91	445	H → L + 1(0.50) H → L(0.38)	0.49	0.68	5.39	−1.40
5	−6.64/−1.83	451	H → L(0.43) H → L + 1(0.44)	1.00	0.90	5.38	−1.37
6	−6.62/−1.84	452	H → L + 1(0.44) H → L(0.41)	1.22	0.94	5.68	−1.06

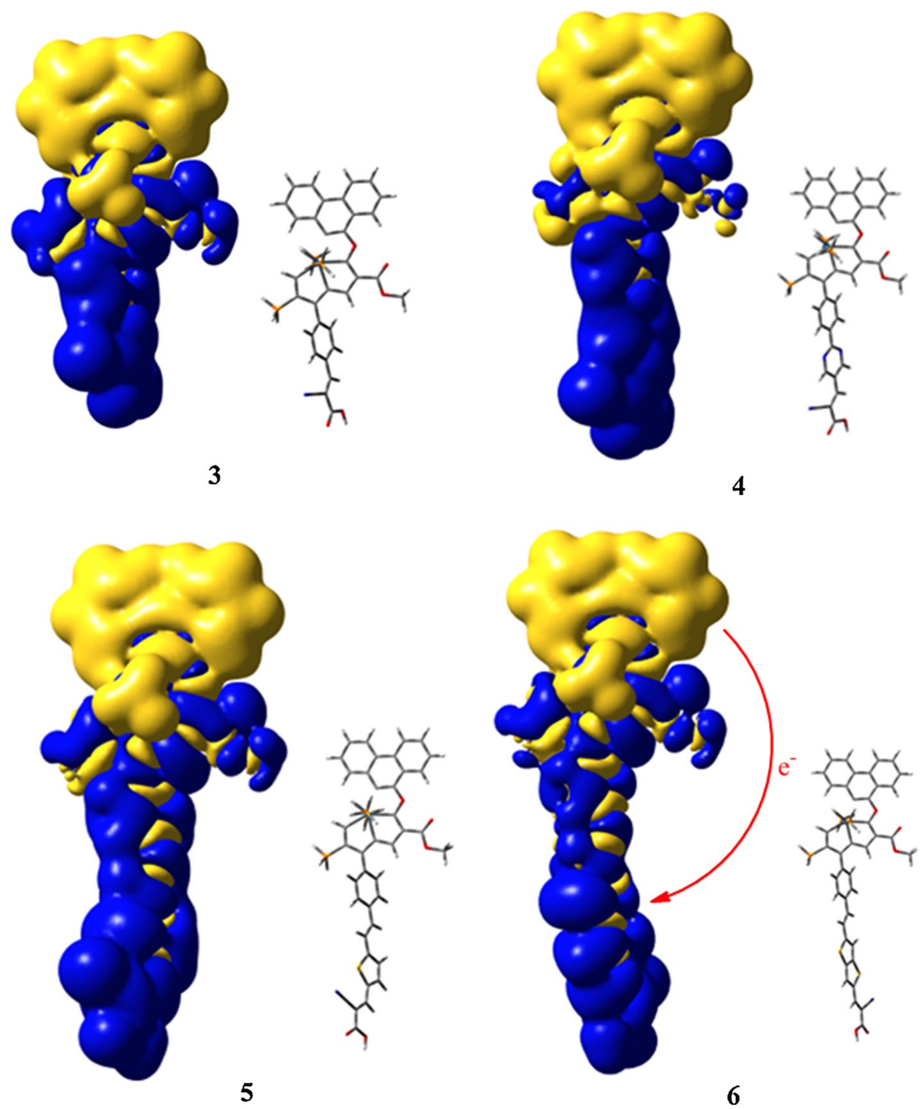

Fig. 4 Electron density differences between the first excited state and the ground state of dyes **3**–**6** (*yellow* and *blue* refer to a decrease and an increase in electron density, respectively; isovalue: 0.00002 au)

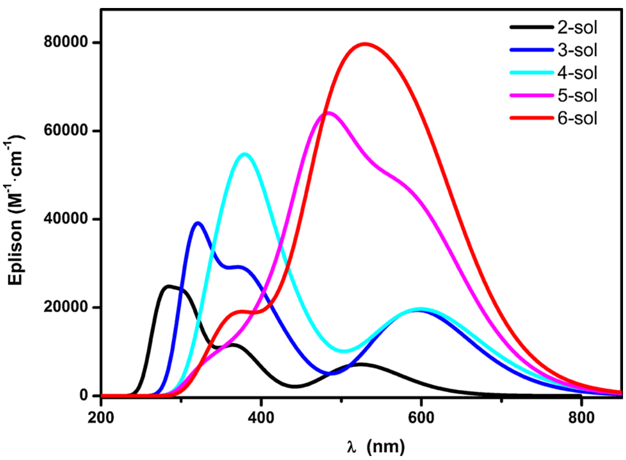

Fig. 5 Predicted absorption spectra of the new designed osmacycle dyes **2**–**6** in the dichloromethane solution by B3LYP

(−4.0 eV vs. vacuum) and HOMO energies are more negative than the potential of I^-/I_3^- redox couple (−4.8 eV vs. vacuum) [29]. Such nice adaptation among corresponding energy levels could ensure effective electron injection of the excited-state dyes and fast regeneration of the oxidized dyes. The dyes **5** and **6** have relatively larger LHE values among them, indicating that the introduction of thiophene and thienothiophene units can enhance the light absorption to a great extent. We note that there is a balance between λ_{max} and ΔG_{inject} under this circumstance which ΔE^{dye} keeps certain values. Hence, the value of ΔG_{inject} can maintain around −1.2 eV with a red-shifted absorption as expected [49]. These results suggest that the dyes **5** and **6** among this series of osmacycles are the most promising candidates for the high-performance photosensitizers.

4 Conclusion

Both B3LYP and CAM-B3LYP calculations on electronic and optical properties of the recently synthesized osmium-bridged tricyclic aromatic complex **2′** show good agreement with the experimental observation, and the calculated CMO-NICS values reveal the strong aromaticity for its relatively high stability. Several new osmacycle dyes, derived from introduction of various π-bridge-conjugated groups based on the complex **2′**, have been designed and characterized theoretically. Calculations show that their electronic and optical properties can well be modulated by incorporating thiophene or thienothiophene bridge unit. The electron density differences between the first excited state and the ground state show much remarkable charge transfer features in the first excited states of dyes **3**–**6**, compared to **2**. In particular, the newly designed osmacycles **5** and **6** were predicted to have excellent charge separation and strong light harvesting ability, as well as large driving forces for electron injection, and they may be potential photosensitizers for high-performance DSSCs.

Acknowledgments This work was supported by the National Science Foundation of China (NSFC) (Grant Nos. 21133007 and 21373164) and the Ministry of Science and Technology (Grant Nos. 2011CB808504 and 2012CB214900). Authors thank Prof. HP Xia and CQ Zhu for useful discussions and dedicated to Professor Guosen Yan on the occasion of his 85th birthday.

References

1. Li B, Wang LD, Kang BN, Wang P, Qiu Y (2006) Sol Energy Mater Sol Cells 90:549–573
2. Hagfeldt A, Boschloo G, Sun L, Kloo L, Pettersson H (2010) Chem Rev 110:6595–6663
3. O'Regan B, Grätzel M (1991) Nature 353:737–740
4. Grätzel M (2001) Nature 414:338–344
5. Grätzel M (2003) J Photochem Photobiol C 4:145–153
6. Nazeeruddin MK, Grätzel M (2007) Struct Bond 123:113–175
7. Ahmad S, Guillen E, Kavan L, Grätzel M, Nazeeruddin MK (2013) Energy Environ Sci 6:3439–3466
8. Hara K, Sayama K, Ohga Y, Shinpo A, Suga S, Arakawa H (2001) Chem Commun 569–570
9. Ito S, Zakeeruddin SM, Humphry-Baker R, Liska P, Charvet R, Comte P, Nazeeruddin MK, Péchy P, Takata M, Miura H, Uchida S, Grätzel M (2006) Adv Mater 18:1202–1205
10. Sayama K, Tsukagoshi S, Mori T, Hara K, Ohga Y, Shinpou A, Abe Y, Suga S, Arakawa H (2003) Sol Energy Mater Sol Cells 80:47–71
11. Tsao HN, Burschka J, Yi C, Kessler F, Nazeeruddin MK, Grätzel M (2011) Energy Environ Sci 4:4921–4924
12. Xu W, Peng B, Chen J, Liang M, Cai F (2008) J Phys Chem B 112:874–880
13. Yella A, Lee HW, Tsao HN, Yi C, Chandiran AK, Nazeeruddin MK, Diau EWG, Yeh CY, Zakeeruddin SM, Grätzel M (2011) Science 334:629–634
14. Kinoshita T, Dy JT, Uchida S, Kubo T, Segawa H (2013) Nat Photonics 7:535–539
15. Nazeeruddin MK, Kay A, Rodicio I, Baker RH, Mueller E, Liska P, Vlachopoulos N, Grätzel M (1993) J Am Chem Soc 115:6382–6390
16. Nazeeruddin MK, Péchy P, Renouard T, Zakeeruddin SM, Baker RH, Comte P, Liska P, Cevey L, Costa E, Shklover V, Spiccia L, Deacon GB, Bignozzi CA, Grätzel M (2001) J Am Chem Soc 123:1613–1624
17. Han L, Islam A, Chen H, Malapaka C, Chiranjeevi B, Zhang S, Yang X, Yanagida M (2012) Energy Environ Sci 5:6057–6060
18. Kandada ARS, Fantacci S, Guarnera S, Polli D, Lanzani G, Angelis FD, Petrozza A (2013) ACS Appl Mater Interfaces 5:4334–4339
19. Altobello S, Argazzi R, Caramori S, Contado C, Fré SD, Rubino P, Choné C, Larramona G, Bignozzi CA (2005) J Am Chem Soc 127:15342–15343
20. Argazzia R, Larramona G, Contado C, Bignozzi CA (2004) J Photoch Photobio A 164:15–21
21. Zhu C, Li S, Luo M, Zhou X, Niu Y, Lin M, Zhu J, Cao Z, Lu X, Wen T, Xie Z, Schleyer PvR, Xia H (2013) Nat Chem 5:698–703
22. Zhu C, Luo M, Zhu Q, Zhu J, Schleyer PVR, Wu J, Lu X, Xia H (2014) Nat Commun 5:3265
23. Zhu C, Zhu Q, Fan J, Zhu J, He X, Cao X, Xia H (2014) Angew Chem Int Ed 53:6232–6236

24. Akimov AV, Neukirch AJ, Prezhdo OV (2013) Chem Rev 113:4496–4565
25. Wang ZS, Yamaguchi T, Sugihara H, Arakawa H (2005) Langmuir 21:4272–4276
26. Al-Sehemi AG, Irfan A, Asiri AM (2012) Theor Chem Acc 131:1199
27. Harris DC, Bertolucci MD (1998) Symmetry and spectroscopy. Dover, New York
28. Katoh R, Furube A, Yoshihara T, Hara K, Fujihashi G, Takano S, Murata S, Arakawa H, Tachiya M (2004) J Phys Chem B 108:4818–4822
29. Asbury J, Wang YQ, Hao E, Ghosh H, Lian T (2001) Res Chem Intermed 27:393–406
30. Jacquemin D, Planchat A, Adamo C, Mennucci B (2012) J Chem Theory Comput 8:2359–2372
31. Fu Y, Liu L, Yu HZ, Wang YM, Guo QX (2005) J Am Chem Soc 127:7227–7234
32. Wang J, Bai FQ, Xia BH, Feng L, Zhang HX, Pan Q (2011) Phys Chem Chem Phys 13:2206–2213
33. Lee C, Yang W, Parr RG (1988) Phys Rev B 37:785–789
34. Becke AD (1993) J Chem Phys 98:5648–5652
35. Frisch MJ, Trucks GW, Schlegel HB, Scuseria GE, Robb MA, Cheeseman JR, Barone GV, Mennucci B, Petersson GA et al (2009) Gaussian 09, revision B.01. Gaussian, Inc, Wallingford
36. Ehlers AW, Böhme M, Dapprich S, Gobbi A, Höllwarth A, Jonas V, Köhler KF, Stegmann R, Veldkamp A, Frenking G (1993) Chem Phys Lett 208:111–114
37. Marenich AV, Cramer CJ, Truhlar DG (2009) J Phys Chem B 113:6378–6396
38. Yanaia T, Tew DP, Handy NC (2004) Chem Phys Lett 393:51–57
39. Dreuw A, Head-Gordon M (2005) Chem Rev 105:4009–4037
40. Autschbach J (2009) Chem Phys Chem 10:1757–1760
41. Zhu C, Liang JX, Cao ZX (2013) J Phys Chem B 117:13388–13395
42. Xu LC, Li J, Shi S, Zheng KC, Ji LN (2008) J Mol Struct Theochem 855:77–81
43. Based on a search of the Cambridge Structural Database, CSD version 5.34 (May 2013)
44. Chen Z, Wannere CS, Corminboeuf C, Puchta R, Schleyer PVR (2005) Chem Rev 105:3842–3888
45. Pelado B, Cruz P, Pedro VG, Barea EM, Langa F (2012) Tetrahedron Lett 53:6665–6669
46. Zhang CR, Liu ZJ, Chen YH, Chen HS, Wu YZ, Yuan LH (2009) J Phys Chem B 899:86–93
47. Guo MY, He RX, Dai Y, Shen W, Li M (2012) J Phys Chem C 116:9166–9179
48. Lu T, "Multiwfn: Multifunctional wavefunction analyzer", Version 3.2.1. http://Multiwfn.codeplex.com
49. Zhang J, Li HB, Sun SL, Geng Y, Wu Y, Su ZM (2012) J Mater Chem 22:568–576